Computational Analysis of Balloon Catheter Behaviour at Variable Inflation Levels

Junke Yao[1], Giorgia Maria Bosi[1], Gaetano Burriesci[1,2], Helge Wurdemann[1]

Abstract— **Aortic valvuloplasty is a minimally invasive procedure for the dilatation of stenotic aortic valves. Rapid ventricular pacing is an established technique for balloon stabilization during this procedure. However, low cardiac output due to the pacing is one of the inherent risks, which is also associated with several potential complications. This paper proposes a numerical modelling approach to understand the effect of different inflation levels of a valvuloplasty balloon catheter on the positional instability caused by a pulsating blood flow. An unstretched balloon catheter model was crimped into a tri-folded configuration and inflated to several levels. Ten different inflation levels were then tested, and a Fluid-Structure Interaction model was built to solve interactions between the balloon and the blood flow modelled in an idealised aortic arch. Our computational results show that the maximum displacement of the balloon catheter increases with the inflation level, with a small step at around 50% inflation and a sharp increase after reaching 85% inflation. This work represents a substantial progress towards the use of simulations to solve the interactions between a balloon catheter and pulsating blood flow.**

I. INTRODUCTION

Aortic stenosis (AS) is a common heart valve disease characterised by pathological thickening of the aortic valve leaflets, usually due to age-related progressive calcification. This condition alters the function of the aortic valve, resulting in a narrowed opening of the valve orifice area and increased systolic pressure within the left ventricle [1]. Transcatheter aortic valve implantation (TAVI) is a minimally invasive intervention that was pioneered in 2002; it is now regarded as the option of preference to treat severe AS in medium to high-risk patients [2]. This approach strongly relies on the use of balloon catheters, either for the valve implantation, as in the case of balloon expandable devices, or as a bridge to TAVI for pre-dilatation, as in the case of balloon aortic valvuloplasty (BAV). The latter has been shown to improve the procedural outcome of the technique, experiencing a substantial increase in its utilisation of more than five-fold in the first decade since TAVI has become a clinical procedure [3]. However, the use of balloon catheters for AS treatments is still assiociated with potential complications that make its application more complex, limiting its widespread. In fact, during BAV and TAVI, pulsating blood flow and energetic cardiac contractility can cause instability of the inflated balloon, which may lead to malposition or cause damage to the surrounding tissues [4], [5]. To counteract this effect, rapid ventricle pacing (RVP) is used to temporarily reduce left ventricular output for balloon stabilisation. Despite its frequent use, RVP is associated with several potential complications, e.g., cardiac perforation, tamponade, and arrhythmia, including ventricular tachycardia [6], [7]. To avoid RVP, recent studies have focused on improving balloon catheter design by investigating small, non-occlusive balloon catheters, or multi-compartment balloon catheters [8], [9]. However, incomplete dilation and substantial backflow from the aorta to the left ventricle through the large central orifice of these balloon catheter necessarily introduces major alterations to the physiological flow and energetic losses. Therefore, it is still necessary to explore alternative solutions easily applicable to commonly used and commercially available balloon catheters, able to avoid the need for RVP and related complications. To do so, the level of balloon inflation that allows for its stabilization during heart systole will be investigated by computational modelling procedures, with inflation and deflation as a starting point for the research.

To this aim, the level of balloon inflation that allows for its stabilization during heart systole was investigated by computational modelling procedures. Numerical simulations have been now established as common and efficient tools to investigate and simulate the mechanical behaviours of medical devices like stents and balloon catheters [10]. Several studies have introduced folded balloons for stent expansion, to investigate different aspects during simulations of the balloon expandable TAVI procedures [11], [12]. However, the majority of numerical studies to date focus on the mechanism and behaviour of stent, with the balloon merely regarded as ancillary to the simulation of stent development [13]. At present, no research has been directly focused on the modelling of the balloon catheter expansion, or interaction between the blood flow and the balloon catheter.

To investigate this issue, in this study a Fluid-Structure Interaction (FSI) model is used to simulate the interplay between a balloon catheter of variable internal volume and the blood flow. First, a 3D model of a commercially available balloon is deflated and crimped to a tri-folded configuration. Then, the effect of different balloon inflation levels on the positional instability caused by the pulsating blood flow is analysed. Finally, the change in position and the fluid dynamics is analysed for different inflation levels.

II. MATERIALS AND METHODS

A structural finite element (FE) model of an Edwards 9350BC23 balloon catheter (Edwards Lifesciences, Irvine, CA, USA) was created based on measurements of the real

[1]J. Yao, G.M. Bosi, G. Burriesci, H. Wurdemann are with the Department of Mechanical Engineering, University College London, UK. `h.wurdemann@ucl.ac.uk`
[2]Gaetano Burriesci is the group leader of Bioengineering at Ri.MED Foundation, Palermo, Italy. `g.burriesci@ucl.ac.uk`
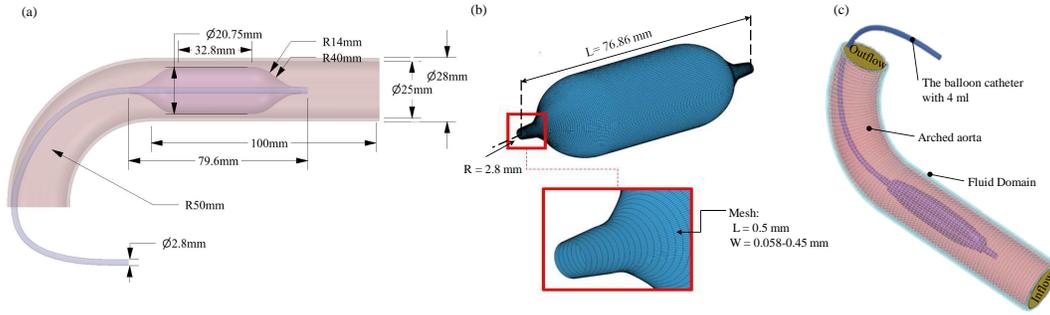
Fig. 1. A valvuloplasty balloon catheter inside an arched idealised aorta. (a) Measurements of the whole structure. (b) Edwards 23 mm balloon FE numerical model. (c) The simulated aortic arch with a balloon catheter inside and the fluid domain; the yellow parts represent inflow and outflow sections.

device, and used to create a tri-folded configuration as the initial state. An idealised tube-like aortic arch was defined as a fluid domain. The balloon catheter model was positioned in the fluid domain and analysed at different levels of inflation adopting an Immersed Boundary FSI coupling approach [14]. The displacement of the balloon produced by the blood flow was quantified for each level of inflation.

A. The physical model

1) The balloon catheter: The over-the-catheter balloon model is identical to previously described models from literature [15] (Fig. 1(a)). The balloon diameter is 20.75 mm in an unstretched state [16], and distal and proximal tapers are attached to the catheter shaft. The total length of the balloon is 79.6 mm with a central cylindrical portion 32.8 mm long. The catheter shaft has a 2.8 mm diameter, and is arched touching the upper inner wall of the aorta (Fig. 1(a)), as shown in x-ray images of the real interventions [17]. The material of the balloon catheter was modelled as isotropic linear-elastic, with Young's modulus equal to 600 MPa, Poisson ratio equal to 0.45 and density equal to 1256 kg=m^3 [18]. The catheter shaft is modelled with 1 GPa Young's modulus, 0.4 Poisson ratio and a density of 1100 kg=m^3 [19].

2) Aorta phantom and blood flow: Researchers have focused on patient-specific aorta phantom development for various cardiovascular applications [20], [21]. Since this study focuses on the systolic duration, when the blood pressures are equal in the ascending aorta and the left ventricle, the balloon catheter can be inserted in a tube-like idealised aorta instead of placing the tip in the ventricle. Therefore, the aortic arch model is generated based on an in-house phantom with a diameter of 25 mm, a thickness of 1.5 mm and an outer diameter of 28 mm. It has a straight section modelling the ascending aorta measuring 100 mm and an arch of 50 mm radius at the axis. The tissue is assumed as a rigid body (Fig. 1(a)). Blood is treated as a Newtonian incompressible fluid with a density of 1060 kg=m^3 and a dynamic viscosity of 4.0×10^{-3} Pa·s [22]. The fluid inside the balloon catheter was assigned the same property as water: a density of 988 kg=m^3, a dynamic viscosity of 0.8×10^{-3} Pa·s and a bulk modulus of 21.5 MPa. The bulk modulus was 1% of the real value to reduce the simulation time [23], though it was verified that this does not affected the analysis results.

The 3D geometrical model of the unfolded and untreated balloon was discretized into 24,600 4-node quadrilateral shell elements with a uniform thickness of 0.3 mm [18] (see Fig. 1(b)). Mesh sensitivity analysis indicated that 150 circumferential elements were adequate to capture the balloon behaviour with the shortest computing time (the differences in the maximum stress and displacement with finer mesh reduced to less than 1%). The shaft catheter was discretized into 2,362 4-node quadrilateral shell elements with a uniform thickness of 0.1 mm. The aorta was discretized into a structured mesh of 14,560 8-node hexahedral elements, with a characteristic dimension of 0.75 to 2 mm. The measurements of the idealised aorta model and how the balloon catheter is inserted inside it are shown in Fig. 1(a). The balloon catheter and the aorta were immersed in a fluid domain, which was discretized into a structured mesh of 85,760 8-node hexahedral Eulerian elements, with a characteristic dimension of 0.54 to 2 mm (Fig. 1(c)).

B. Numerical simulations

1) Simulation 1 - Balloon deflation: To create the geometry of the tri-folded crimped balloon, two distinct steps were taken for deflation and crimping, with the two tapered ends constrained for three directions during the whole process. The first step involved a linear pressure with the absolute value increasing to 0.1 MPa within 10 ms, resulting in a suction pressure of about 1 atm distributed. The three nodes set every 120° on the balloon circumference were constrained along the radial direction of the balloon, ensuring the balloon model to deflate into a star-shaped, tri-wing configuration, similar to that observed experimentally. Then, 12 rigid planes serve to pleat the three balloon wings in the same direction until their diameter is reduced to 9 mm [18], replicating the function of the segments of the iris mechanism used in TAVI application. Self-contact interactions and contact pairs between the balloon and planes were modelled by penalty formulations considering shell thickness.

2) Simulation 2 - Balloon inflation: The 3D tri-folded balloon model was used to investigate the inflation process by importing the unloaded configuration from the simulation 1. Structural FE analysis was used to apply pressure on the surface of the balloon membrane until it reached the nominal diameter of the balloon through an implicit solver. The two ends were constrained in three directions.
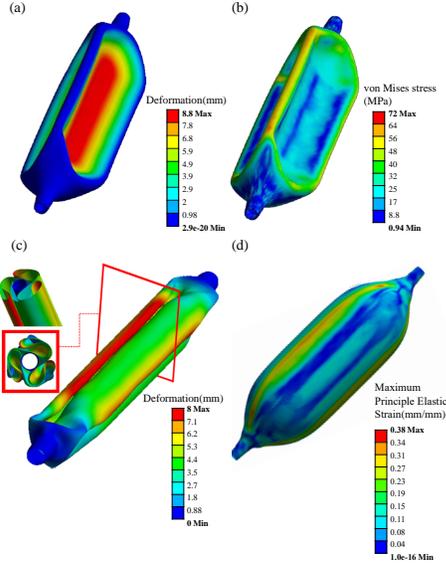
Fig. 2. The deflation and inflation results of the balloon catheter. (a) The distribution of deformation of the balloon after pressurization. (b) The distribution of von Mises stress after pressurization. (c) Crimping deformation distribution where the cross-section is three-wings folded. (d) The Maximum principle elastic strain of the inflated balloon model.

3) Simulation 3 - FSI with blood flow: The unloaded balloon models at different inflation levels were imported into the FSI model. The inlet boundary condition used for the fluid domain consisted in a parabolic velocity profile with maximum value equal of 1.3 $\frac{m}{s}$ at the systole peak [24], [25].

FEM simulations were run through Ansys v19.0 (ANSYS Inc., Canonsburg, USA). FSI simulations were run through a125 commercial explicit FE solver LS-DYNA 971 (LSTC, Livermore, USA). The 3D geometrical models were generated using Ansys SpaceClaim meshed by HyperMesh 2019. Simulations were performed on an Intel CORE i9-10900K CPU, 3.7GHz, 64GB (Intel Corporation, Santa Clara, USA).

III. COMPUTATIONAL RESULTS

A. Simulation 1: The tri-folded crimped balloon model

To develop a balloon catheter model with different levels of inflation, the first step consisted in deflating the un-stretched balloon model to a tri-folded configuration called the folding process. The computational time for the dry balloon folding simulation was 11 hours. To ensure the inertial forces were negligible and no unrealistic dynamic effect occurs throughout the simulation of a quasi-static analysis when using the explicit solver, the ratio of kinetic energy to the total internal energy was maintained lower than 5% during the simulation time. As can be seen in Fig. 2(a), there is a significant deformation of the balloon catheter, resulting in the balloon adopting a star shape. The maximum von Mises stress is 72 MPa at the end of the simulation; while considering the entire simulation time, the maximum value is 100.59 MPa, which occurs at 0.008 s in Fig. 2(b). During the crimping step, the larger deformation is shown to reduce the diameter to 9 mm (Fig. 2(c)). The resulting

tri-folded balloon model has an inner volume of 2.16 ml as the potential residual medium inside the balloon cavity.

B. Simulation 2: Inflation procedure of the balloon model

FEM analysis of the balloon inflation was characterized by a computational time of 3.5 hours, with a simulation time of 1.46 seconds. During the first 0.2 seconds, the three wings of the balloon unfold gradually, the balloon then expands within 0.01 seconds. The balloon diameter increases to 23.3 mm on an approximately linear scale. The von Mises stress and deformation peak values during the simulation have a similar plot, which increases gradually except for a significant increase around 0.75 MPa. In Fig. 2(d), the element located at the folded edges and folded dents becomes stretched more than other elements when the level of inflation increases. During the expansion process, the balloon diameter first increases from 9 to 12.2 mm at 0.2 s before increasing to 20.77 mm at 0.4 s; it finally reaches 23 mm at 1.3 s. During the inflation, 33 planes are used to measure the horizontal maximum diameter of the balloon (Fig. 3(a) and (b)) and the deformed geometry models are exported to measure volume. There is no severe distortion, particularly at the tapering end of the balloon, which is exposed to high stresses.

C. Simulation 3: Balloon catheter models in fluid environment

The computational time of one simulation is 170-190 hours, which includes one specific inflation level of the balloon catheter. Ten balloon catheter models containing from 4 to 20 ml with a 2 ml increment, plus a balloon with 21 ml are simulated to determine their maximum displacement.

A sectional view of the model shows the flow velocity distribution when it reaches the highest value (1.225 $\frac{m}{s}$) at 0.9 s (Fig. 4(a)). From the inlet interface section, the flow velocity distribution, set with a parabolic profile at the start, takes a more triangular distribution as effect of the balloon. In Fig. 4(b), it can be observed that the fluid velocity within the aortic arch increases close to the external wall. When 4, 6 and 8 ml models are inserted, the flow passing the balloons results in a peak velocity of about 0.3 $\frac{m}{s}$ (at 0.9 s). However, when the volume reaches 10 ml, the maximum flow velocity reduces to less than 0.15 $\frac{m}{s}$ (at 0.9 s). When the balloon model is inflated to the maximum volume of 21 ml, the displacement of the balloon almost doubles compared to 20 ml inflation. Based on Fig. 4(c), the maximum displacement of the 4, 6 and 8 ml balloon are 1.22, 1.48 and 1.81 mm, respectively. Thus, the plot from 4 to 8 ml shows a relatively low slope trend. When the volume increases from 8 to 10 ml, the displacement shows a jump and increases to 3.24 mm. For 12 to 18 ml inflation levels, the maximum displacement continues to increase from 3.76 to 5.08 mm, but the slope of the increment decreases. The maximum displacement jumps to 5.08 mm, but the slope of the increment decreases. The maximum displacement jumps to 9.55 mm for the 20 ml balloon, and increases to 18.47 mm when the 21 ml balloon catheter is inserted with a 0.88 cross-section area ratio (CSAR).
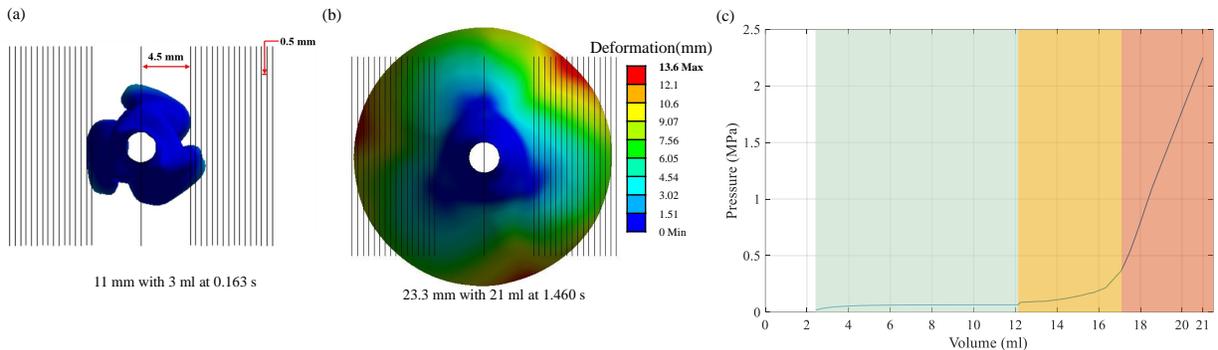
Fig. 3. The results of the deformation of a balloon catheter during inflation. (a) Balloon inflation at 0.163 s when the maximum horizontal distance increases to 11 mm and volume increases to 3 ml. (b) Balloon inflation at 1.46 s when the maximum horizontal distance increases to 23.4 mm and volume increases to 21 ml. (c) The pressure-volume curve of the numerical balloon inflation process, where the green region shows a plateau; the yellow part illustrates the start of the increase; the red area demonstrates the sharp increment.

IV. DISCUSSION

The FE numerical model of the balloon catheter used in this study focused on the balloon's configuration and shape change during inflation and deflation, allowing a detailed description of its geometry. In a study by Geith *et al.* regarding the balloon catheter model with experimental validation, it is mentioned that the von Mises stress during the folding process was more than 100 MPa [26], where the maximum von Mises stress of the pressurization process was similar, with a value of 100.57 MPa. Both Geith's work and our current study found that the greatest von Mises stress occurred at the kink point during the crimping procedure. The cross-section balloon model quickly changed from tri-folded to cylindrical when around one atmosphere pressure was applied on the inner surface; the maximum horizontal diameter of the balloon then increased slowly with the linear increase of applied pressure.

In addition, the pressure-volume curve from the simulation (Fig. 3(c)) shows a similar trend with the pressure-volume curve from experimental data in the previous study [16], where the pressure plateaus, followed by a sharp increment until the volume reaches 21 ml.

FSI models simulated balloons with different inflation levels. The maximum displacement shows two jumps when increasing the inflation level between 8 and 10 ml and between 18 and 20 ml. When the balloon reaches its maximum volume (21 ml), the displacement becomes more than half of the effective cylindrical length of the balloon. The sharp increase of the balloon displacement after 10 ml first and then after 18 ml, suggests that there is a threshold volume that allows the balloon to create significant displacement, and another threshold volume forces the balloon's displacement to have an abrupt growth in 4(c). By looking at the small value (<1.5 mm) of balloon displacement when the balloon is inflated less than a volume of 10 ml, it can be inferred that the balloon in this situation is relatively stable. Therefore, if the balloon is periodically deflated to a 'safe volume' (i.e. <10 ml) during systole, and inflated to its required volume to achieve valve expansion during diastole, it is possible to achieve stabilisation avoiding the complications caused by RVP and reducing the length and complexity of the procedure.

From a technical standpoint, the main goal of this work is to advance the state of the art in aortic valvuloplasty balloon catheter FSI modelling, which will allow the identification of novel tools supporting the treatment of clinically relevant problems and the design of enhanced medical devices. To the authors' knowledge, this model is the first attempt to apply FSI modelling with strong coupling to the simulation of a balloon catheter and aorta with realistic loading conditions.

V. CONCLUSION

In the present study, a successful workflow for FE of the balloon catheter deflation and inflation procedures and FSI simulations to analyse the interaction between a balloon and blood flow inside the idealised aorta were presented. The workflow was composed of five steps: (a) implementing detailed geometry of the balloon including the tapered-end attached to the catheter; (b) deflating the balloon by pressurization and crimping to an unsymmetrical, star-like configuration; (c) using an implicit solver for the quasi-static problem of the balloon inflation; and (d) obtaining balloon catheter models with different levels of inflation according to internal volume values; (e) applying parabolic profile velocity to the blood flow in the aorta to simulate interaction with balloon catheter models in the FSI simulation. Ultimately, the FSI simulation for these balloon catheter models demonstrates that the displacement of the balloon experiences a jump at around 50% inflation level and increases sharply after 85% inflation. These findings provide a potential insight for using the balloon catheter avoiding RVP during valvuloplasty by pacing the balloon inflation, rather than the patient's heart. FSI modelling could also prove beneficial in determining the behaviour of balloon catheters under the different pressure conditions found in the left ventricular outflow tract.

REFERENCES

[1] K. Amrit, J. T. Jeremy, and V. T. Nkomo, "Management of patients with aortic valve stenosis," *Mayo Clinic Proceedings*, vol. 93, no. 4, pp. 488–508, 2018.
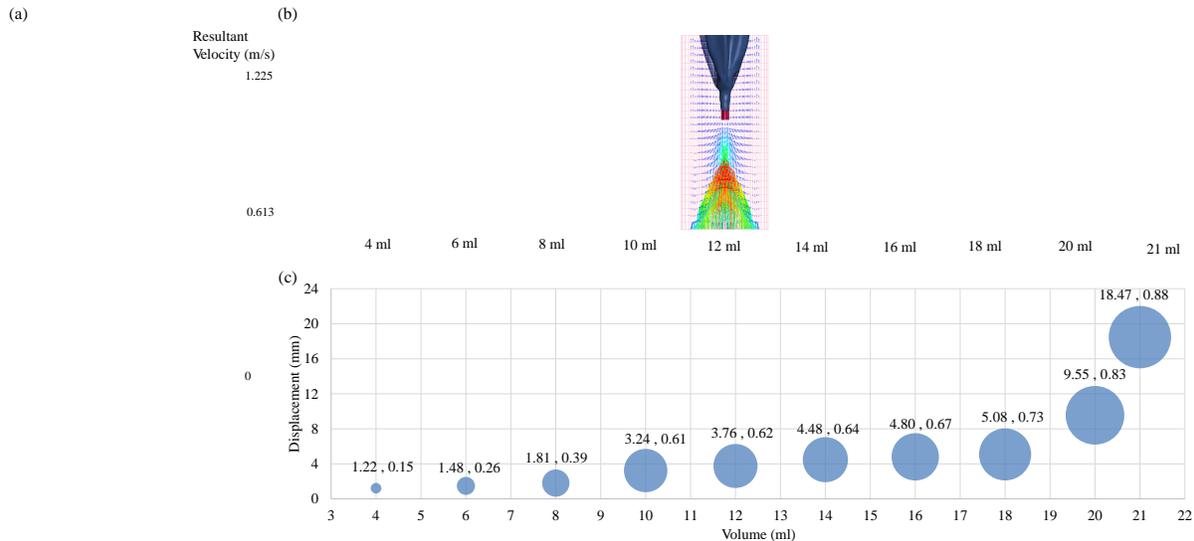
Fig. 4. The results of Fluid-Structure Interaction simulation. (a) The cross-section of the velocity distribution of the flow inside the aorta with an internal balloon volume of 21 ml at 0.9 s. (b) The velocity arrow distribution for ten inflation level models at 0.9 s, which shares the same legend with (a). (c) The plot of the maximum displacement of the balloon catheters and the volume, with the area ratio between the cross section of the balloon and the aorta.

[2] A. Cribier *et al.*, "Percutaneous Transcatheter Implantation of an Aortic Valve Prosthesis for Calcific Aortic Stenosis," *Circulation*, vol. 106, no. 24, pp. 3006–3008, 2002.

[3] T. R. Keeble, A. Khokhar, M. M. Akhtar, A. Mathur, R. Weerackody, and S. Kennon, "Percutaneous balloon aortic valvuloplasty in the era of transcatheter aortic valve implantation: a narrative review," *Open Heart*, vol. 3, no. 2, p. e000421, 2016.

[4] C. Witzke *et al.*, "Impact of rapid ventricular pacing during percutaneous balloon aortic valvuloplasty in patients with critical aortic stenosis: should we be using it?" *Catheterization and Cardiovascular Interventions*, vol. 75, no. 3, pp. 444–452, 2010.

[5] I. Daehnert, C. Rotzsch, M. Wiener, and P. Schneider, "Rapid right ventricular pacing is an alternative to adenosine in catheter interventional procedures for congenital heart disease," *Heart*, vol. 90, no. 9, pp. 1047–1050, 2004.

[6] C. Mehta, S. Shebani, V. Grech, and J. Degiovanni, "How to achieve balloon stability in aortic valvuloplasty using rapid ventricular pacing," *Images in Paediatric Cardiology*, vol. 6, no. 4, pp. 31–37, 2004.

[7] B. M. Jones *et al.*, "Rapid ventricular pacing during transcatheter valve procedures using an internal device and programmer: A demonstration of feasibility," *Catheterization and Cardiovascular Interventions*, vol. 95, no. 5, pp. 1042–1048, 2020.

[8] A. Shivaraju *et al.*, "Aortic Valve Predilatation with a Small Balloon, without Rapid Pacing, prior to Transfemoral Transcatheter Aortic Valve Replacement," *BioMed Research International*, vol. 2018, no. February 2014, pp. 2–7, 2018.

[9] S. Toggweiler *et al.*, "Simplifying transfemoral acurate neo implantation using the trueflow nonocclusive balloon catheter," *Catheterization and Cardiovascular Interventions*, vol. 96, no. 6, pp. E640–E645, 2020.

[10] D. Martin and F. J.Boyle, "Computational structural modelling of coronary stent deployment: a review," *Computer Methods in Biomechanics and Biomedical Engineering*, vol. 14, no. 4, pp. 331–348, 2011.

[11] M. Bianchi *et al.*, "Effect of Balloon-Expandable Transcatheter Aortic Valve Replacement Positioning: A Patient-Specific Numerical Model," *Artificial Organs*, vol. 40, no. 12, pp. E292–E304, 2016.

[12] G. M. Bosi *et al.*, "Population-specific material properties of the implantation site for transcatheter aortic valve replacement finite element simulations," *Journal of Biomechanics*, vol. 71, pp. 236–244, 2018.

[13] S. Morlacchi and F. Migliavacca, "Modeling Stented Coronary Arteries: Where We are, Where to Go," *Annals of Biomedical Engineering*, vol. 41, no. 7, pp. 1428–1444, 2013.

[14] C. S. Peskin, "Flow patterns around heart valves: A numerical method," *Journal of Computational Physics*, vol. 10, no. 2, pp. 252–271, 1972.

[15] B. Benedetta *et al.*, "Numerical model of a valvuloplasty balloon: in

vitro validation in a rapid-prototyped phantom." *BioMed Eng OnLine*, vol. 15, no. 37, pp. 1–6, 2016.

[16] A. Palombi *et al.*, "Sizing the aortic annulus with a robotised, commercially available soft balloon catheter: In vitro study on idealised phantoms," *IEEE International Conference on Robotics and Automation*, vol. 2019-May, 2019.

[17] I. Vernikouskaya *et al.*, "Image-guidance for transcatheter aortic valve implantation (tavi) and cerebral embolic protection," *International Journal of Cardiology*, vol. 249, pp. 90–95, 2017.

[18] F. Sturla *et al.*, "Impact of different aortic valve calcification patterns on the outcome of transcatheter aortic valve implantation: A finite element study," *Journal of Biomechanics*, vol. 49, no. 12, pp. 2520–2530, 2016.

[19] D. Martin and F. Boyle, "Sequential Structural and Fluid Dynamics Analysis of Balloon-Expandable Coronary Stents: A Multivariable Statistical Analysis," *Cardiovascular Engineering and Technology*, vol. 6, no. 3, pp. 314–328, 2015.

[20] A. Gallarello *et al.*, "Patient-Specific Aortic Phantom With Tunable Compliance," *Journal of Engineering and Science in Medical Diagnostics and Therapy*, vol. 2, no. 4, 2019.

[21] G. Annio *et al.*, "Low-Cost Fabrication of Polyvinyl Alcohol-Based Personalized Vascular Phantoms for In Vitro Hemodynamic Studies: Three Applications," *Journal of Engineering and Science in Medical Diagnostics and Therapy*, vol. 3, no. 3, 2020.

[22] Y. Bazilevs, J. Gohean, T. Hughes, R. Moser, and Y. Zhang, "Patient-specific isogeometric fluid–structure interaction analysis of thoracic aortic blood flow due to implantation of the jarvik 2000 left ventricular assist device," *Computer Methods in Applied Mechanics and Engineering*, vol. 198, no. 45-46, pp. 3534–3550, 2009.

[23] F. Sturla, E. Votta, M. Stevanella, C. A. Conti, and A. Redaelli, "Impact of modeling fluid–structure interaction in the computational analysis of aortic root biomechanics," *Medical Engineering and Physics*, vol. 35, no. 12, pp. 1721–1730, 2013.

[24] K. Cao and P. Sucosky, "Effect of bicuspid aortic valve cusp fusion on aorta wall shear stress: Preliminary computational assessment and implication for aortic dilation," *World Journal of Cardiovascular Diseases*, vol. 5, pp. 129–140, 05 2015.

[25] O. Smadi, I. Hassan, P. Pibarot, and L. Kadem, "Numerical and experimental investigations of pulsatile blood flow pattern through a dysfunctional mechanical heart valve," *Journal of Biomechanics*, vol. 43, no. 8, pp. 1565–1572, 2010.

[26] M. A. Geith, K. Swidergal, B. Hochholdinger, T. G. Schratzenstaller, M. Wagner, and G. A. Holzapfel, "On the importance of modeling balloon folding, pleating, and stent crimping: An FE study comparing experimental inflation tests," *International Journal for Numerical Methods in Biomedical Engineering*, vol. 35, no. 11, pp. 1–19, 2019.